Pygmy dipole resonance as a constraint on the neutron skin of heavy nuclei

J. Piekarewicz
Department of Physics, Florida State University, Tallahassee, Florida 32306, USA
(Received 11 February 2006; published 26 April 2006)

The isotopic dependence of the isovector Pygmy dipole response in tin is studied within the framework of the relativistic random-phase approximation. Regarded as an oscillation of the neutron skin against the isospin-symmetric core, the pygmy dipole resonance may place important constraints on the neutron skin of heavy nuclei and, as a result, on the equation of state of neutron-rich matter. The present study centers around two questions. First, is there a strong correlation between the development of a neutron skin and the emergence of low-energy isovector dipole strength? Second, could one use the recently measured Pygmy dipole resonance in ^{130}Sn and ^{132}Sn to discriminate among theoretical models? For the first question we found that although a strong correlation between the neutron skin and the Pygmy dipole resonance exists, a mild anticorrelation develops beyond ^{120}Sn. The answer to the second question suggests that models with overly large neutron skins—and thus stiff symmetry energies—are in conflict with experiment.

DOI: 10.1103/PhysRevC.73.044325 PACS number(s): 21.10.Re, 21.60.Jz

I. INTRODUCTION

The accurate determination of the neutron radius of a heavy nucleus remains an unsolved nuclear-structure problem. The search for this fundamental observable has been recently reinvigorated because of its far-reaching influence on a host of interesting and seemingly unrelated observables. For example, a correlation has been found between the neutron radius of ^{208}Pb and the binding energy of the valence neutrons in neutron-rich nuclei: models with small neutron radii reach the neutron drip line sooner than those with larger radii [1]. Further, an additional correlation was found between the neutron radius of ^{208}Pb and the neutron radius of other heavy nuclei. This suggests that the measurement of the neutron radius of a single heavy nucleus could determine, or at least place strong constraints on, the neutron radius of a variety of nuclei. This could provide a boost to the atomic parity-violation program [2]. Many other physical observables also display a strong correlation with the neutron radius of ^{208}Pb. These include the equation of state of neutron-rich matter [3], isospin diffusion in heavy-ion collisions [4–6], and the structure and dynamics of neutrons stars [7–11].

Attempts at mapping the neutron distribution have traditionally relied on strongly interacting probes. Although highly mature and successful, it is unlikely that the hadronic program will ever attain the precision status that the electroweak program enjoys. This is because of the large and controversial uncertainties in the reaction mechanism [12,13]. The mismatch in our knowledge of the proton radius in ^{208}Pb relative to that of the neutron radius provides a striking example of the current situation: although the charge radius of ^{208}Pb is known to better than 0.001 fm [14], realistic estimates place the uncertainty in the neutron radius at about 0.2 fm [15].

The enormously successful parity-violating program at the Jefferson Laboratory [16,17] provides an attractive electroweak alternative to the hadronic program. Indeed, the Parity Radius Experiment (PREX) at the Jefferson Laboratory aims to measure the neutron radius of ^{208}Pb accurately (to within 0.05 fm) and model independently via parity-violating electron scattering [15]. Parity violation at low momentum transfers is particularly sensitive to the neutron density because the Z^0 boson couples primarily to neutrons. Moreover, the parity-violating asymmetry, although small, can be interpreted with as much confidence as conventional electromagnetic scattering experiments. PREX will provide a unique observational constraint on the thickness of the neutron skin of a heavy nucleus. We note that since first proposed in 1999, many of the technical difficulties intrinsic to such a challenging experiment have been met. For example, during the recent activity at the Hall A Proton Parity Experiment (HAPPEX), significant progress was made in controlling helicity correlated errors [18]. Other technical problems are currently being solved—such as the designed of a new septum magnet—and a specific timeline has been provided to solve all remaining problems within the next two years [18].

While this important experiment gets off the ground, a significant effort has been devoted to constrain the neutron radius of a heavy nucleus by alternative means. One such effort uses nuclear giant resonances to constrain bulk properties of infinite nuclear matter, such as the compression modulus and the symmetry energy [19–23]. Knowledge of the density dependence of the symmetry energy places important constraints on the neutron skin of heavy nuclei. Indeed, the slope of the symmetry energy—a quantity related to the pressure of neutron-rich matter—has been shown to be strongly correlated to the neutron radius of heavy nuclei [3]. Yet the reliance on nuclear excitations stems from the inability of existent ground-state observables to constrain the density dependence of the symmetry energy. Although accurately calibrated models reproduce a variety of ground-state observables, they still generate a large spread in the neutron skin of heavy nuclei [3,24].

In this presentation we focus on the "pygmy" dipole resonance (PDR), a soft nuclear mode that has the promise of constraining the neutron skin of heavy nuclei. The timing

of this work is motivated by a pioneering experiment that has identified low-energy isovector dipole strength in two unstable neutron-rich isotopes: ^{130}Sn and ^{132}Sn [25]. Pictured as an oscillation of the neutron skin of the neutron-rich nucleus against the isospin-symmetric core, the emergence of low-energy strength is expected to follow closely the development of the neutron skin. The goals of the present manuscript are therefore twofold: (a) to use the isotopic chain in tin to search for a correlation between the development of a neutron skin and the emergence of low-energy isovector dipole strength and (b) to use the recent experimental data [25] to discriminate among theoretical models that, although accurately calibrated, yield different predictions for the neutron skin of heavy nuclei.

Theoretical studies of the pygmy dipole resonance are not new. The possible existence of a new type of dipole oscillation in which the neutron skin vibrates against the isospin-symmetric core dates back to the early 1990s [26,27]. Shortly after, sophisticated mean-field (MF) plus random-phase-approximation (RPA) approaches were developed and used to predict the distribution of low-energy isovector dipole strength on a variety of neutron-rich nuclei [28–31]. More recently, some of these models have attained a level of sophistication that surpass MF+RPA approaches by incorporation such effects as pairing correlations and/or the coupling to more complex configurations [32–35].

In the present contribution we compare for the first time relativistic MF+RPA calculations against the experimental data of Ref. [25]. The experimental data is used to discriminate among accurately calibrated models having a different density dependence for the symmetry energy, such as NL3 [36,37] and FSUGold [38]. The self-consistent MF+RPA approach employed here neglects both pairing correlations and the coupling to more complex configurations. Yet by direct comparison to some of the most recent studies [32–35]—or by the authors own admission—these effects do not affect the main conclusions of the present work.

The manuscript has been organized as follows. In Sec. II we introduce some of the most basic details of the MF+RPA formalism. For a more comprehensive discussion the reader is referred to Ref. [39]. In Sec. III results for the distribution of isovector dipole strength in the neutron-even Sn-isotopes are presented. In the same section we discuss the various effects that may be used to elucidate the neutron skin of heavy nuclei and, correspondingly, the equation of state of neutron-rich matter. We close by offering our conclusions in Sec. IV.

II. FORMALISM

The starting point for the calculation of the nuclear response is an interacting Lagrangian density of the following form:

$$\begin{aligned}\mathcal{L}_{\rm int} = \bar{\psi}\left[g_s\phi - \left(g_v V_\mu + \frac{g_\rho}{2}\boldsymbol{\tau}\cdot\mathbf{b}_\mu + \frac{e}{2}(1+\tau_3)A_\mu\right)\gamma^\mu\right]\psi \\ - \frac{\kappa}{3!}(g_s\phi)^3 - \frac{\lambda}{4!}(g_s\phi)^4 + \frac{\zeta}{4!}\left(g_v^2 V_\mu V^\mu\right)^2 \\ + \Lambda_v\left(g_\rho^2\,\mathbf{b}_\mu\cdot\mathbf{b}^\mu\right)\left(g_v^2 V_\mu V^\mu\right). \qquad (1)\end{aligned}$$

The Lagrangian density includes an isodoublet nucleon field (ψ) interacting via the exchange of two isoscalar mesons, a scalar (ϕ) and a vector (V^μ), one isovector meson (b^μ), and the photon (A^μ) [40,41]. In addition to meson-nucleon interactions the Lagrangian density is supplemented by four nonlinear meson interactions with coupling constants denoted by κ, λ, ζ, and Λ_v. The first three of these terms are responsible for a softening of the equation of state of symmetric nuclear matter—at both normal and high densities [42]. The last coupling constant (Λ_v) induces isoscalar-isovector mixing and is responsible for modifying the density dependence of the symmetry energy [7,8]. As a result of the strong correlation between the pressure of neutron-rich matter and the neutron radius of heavy nuclei [3,24], Λ_v may also be used to modify the neutron radius of heavy nuclei.

A. Ground-state properties

The initial step in the study of nuclear excitations is the calculation of ground-state properties. This is done by solving the equations of motion associated with the above Lagrangian self-consistently in a relativistic mean-field approximation. What emerges from such a calculation is a set of binding energies, a corresponding set of wave functions, and a self-consistent mean-field potential. From these wave functions, ground-state densities and all their corresponding moments (e.g., root-mean-square radii) may be extracted.

A typical example of such a mean-field procedure is provided in Fig. 1, where point proton and point neutron root-mean-square radii are displayed for all neutron-even isotopes of tin ranging from the doubly magic nucleus ^{100}Sn to the doubly magic nucleus ^{132}Sn. When available, these calculations are compared against experimental data. The same information alongside ground-state energies is displayed in Table I. Two accurately calibrated parameter sets—NL3 [36, 37] and FSUGold [38]—were employed in the calculation. Masses and coupling constants for these two models have been listed in Table II. Note that for the NL3 parameter set, both ζ and Λ_v have been set equal to zero. The absence of a quartic

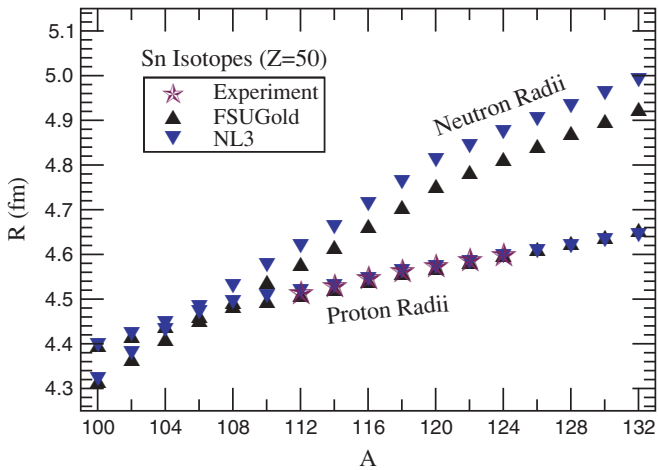

FIG. 1. (Color online) Proton and neutron root-mean-square radii for a variety of even-neutron Sn isotopes computed in a relativistic mean-field approximation using the FSUGold and NL3 parameter sets. Experimental data, when available, are from Ref. [43].

TABLE I. Binding energy per nucleon, proton root-mean-square radii, and neutron-skin thickness for a variety of even-neutron Sn isotopes computed in a relativistic mean-field approximation using the FSUGold and NL3 parameter sets. A center-of-mass correction of the form $(3/4)41A^{-4/3}$ has been applied to the binding energy per nucleon. Experimental data are from Refs. [43,44].

A	FSUGold			NL3			Experiment	
	B/A (MeV)	R_p (fm)	$R_n - R_p$ (fm)	B/A (MeV)	R_p (fm)	$R_n - R_p$ (fm)	B/A (MeV)	R_p (fm)
100	8.244	4.397	−0.080	8.284	4.397	−0.076	8.249(4)	—
102	8.293	4.419	−0.053	8.312	4.421	−0.044	8.323(4)	—
104	8.345	4.440	−0.030	8.355	4.445	−0.015	8.383(2)	—
106	8.399	4.462	−0.009	8.396	4.469	0.011	8.433(1)	—
108	8.456	4.484	0.010	8.440	4.493	0.035	8.468	—
110	8.470	4.497	0.041	8.455	4.575	0.070	8.496	—
112	8.487	4.510	0.069	8.474	4.517	0.102	8.514	4.516
114	8.506	4.523	0.094	8.495	4.528	0.133	8.523	4.532
116	8.496	4.541	0.122	8.486	4.545	0.167	8.523	4.549
118	8.490	4.559	0.148	8.480	4.561	0.199	8.517	4.564
120	8.477	4.570	0.182	8.468	4.572	0.238	8.505	4.577
122	8.447	4.584	0.200	8.446	4.583	0.259	8.488	4.589
124	8.420	4.598	0.216	8.425	4.595	0.278	8.467	4.601
126	8.396	4.612	0.231	8.407	4.607	0.296	8.444	—
128	8.375	4.626	0.245	8.391	4.619	0.314	8.417	—
130	8.356	4.640	0.259	8.377	4.631	0.330	8.388	—
132	8.334	4.654	0.271	8.365	4.644	0.346	8.355	—

vector coupling term (ζ) should not come as a surprise, as the variety of ground-state observables employed in the calibration procedure (such as binding energies and charge radii) are insensitive to the high-density component of the equation of state. Yet the absence of the isoscalar-isovector coupling Λ_v—or any other term that may change the density dependence of the symmetry energy—is significant. It suggests that despite the vast amount of accurate ground-state data collected over the years, it is not possible at present to pin down the neutron radius of even a single heavy nucleus. Both Fig. 1 and Table I indicate that, when a comparison is possible, the agreement between theory and experiment is excellent. Yet these two models, although accurately calibrated, predict vastly different neutron radii for the neutron-rich isotopes.

B. Isovector dipole response

The calculations presented here follow closely the formalism developed in much greater detail in Ref. [39]. It is, however, advantageous to provide a brief summary of the main points of the approach. The isovector dipole response will be extracted from the timelike component of the polarization tensor. Consistent with the assumption of a mean-field ground state, the polarization tensor is computed using a relativistic MF+RPA formalism. Moreover, the residual particle-hole interaction is consistent with the mean-field potential employed to generate the ground state. This, by itself and with nothing else, guarantees both the decoupling of the spurious strength from the RPA response as well as the conservation of the vector current [39,45].

To start, we introduce the most general polarization tensor that is defined in terms of a time-ordered product of two arbitrary nucleon currents:

$$i\Pi^{\alpha\beta}(x, y) = \langle \Psi_0 | T[\hat{J}^{\alpha}(x)\hat{J}^{\beta}(y)] | \Psi_0 \rangle. \tag{2}$$

Here Ψ_0 denotes the exact nuclear ground state and $\hat{J}^{\alpha}(x)$ is a one-body current operator of the form

$$\hat{J}^{\alpha}(x) = \bar{\psi}(x)\Gamma^{\alpha}\psi(x), \tag{3}$$

where Γ^{α} is a matrix having an arbitrary Dirac and isospin structure. In the particular case of nuclear excitations of isovector dipole character, a simple operator of the following form will be used to drive the transition:

$$\Gamma^{\alpha} \rightarrow \Gamma^{0}_{3} \equiv \gamma^{0}\tau_3, \tag{4}$$

where τ_3 is a 2×2 isospin matrix and for the γ matrices we have adopted the convention of Ref. [46]. Finally, because of the invariance under time translation, it is convenient to rewrite the polarization tensor in terms of the excitation energy ω as

TABLE II. Model parameters used in the calculations. The parameter κ and the inverse scalar range m_s are given in MeV. The nucleon, ω, and ρ masses are kept fixed at $M = 939$ MeV, $m_\omega = 782.5$ MeV, and $m_\rho = 763$ MeV, respectively.

Model	m_s	g_s^2	g_v^2	g_ρ^2	κ	λ	ζ	Λ_v
NL3	508.1940	104.3871	165.5854	79.6000	3.8599	−0.0159	0.0000	0.0000
FSUGold	491.5000	112.1996	204.5469	138.4701	1.4203	+0.0238	0.0600	0.0300

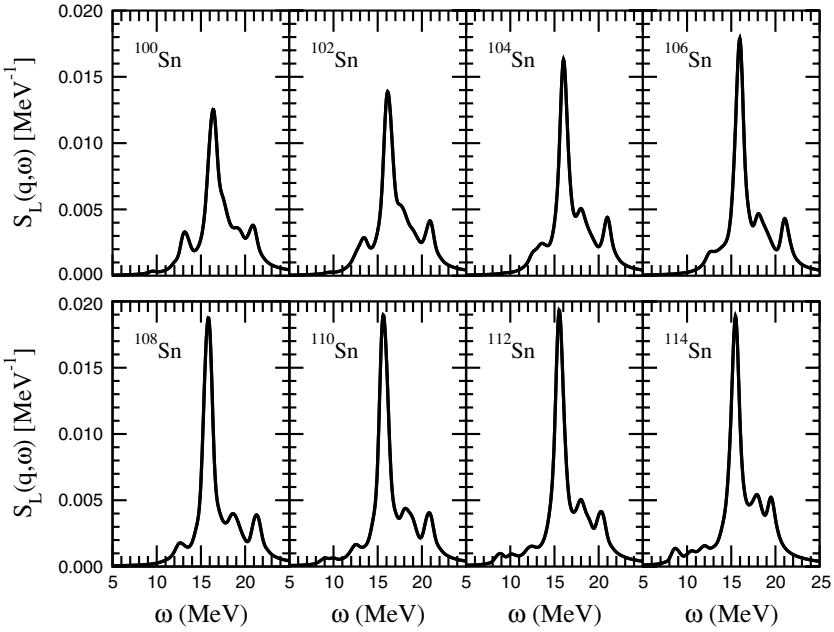

FIG. 2. Distribution of isovector dipole strength for all neutron-even tin isotopes from ^{100}Sn to ^{114}Sn at a momentum transfer of $q = 0.018$ fm^{-1}. All calculations include a small artificial width of $\eta = 0.5$ MeV and use the FSUGold parameter set [38].

follows:

$$\Pi^{\alpha\beta}(x, y) = \int_{-\infty}^{\infty} \frac{d\omega}{2\pi} e^{-i\omega(x^0 - y^0)} \Pi^{\alpha\beta}(\mathbf{x}, \mathbf{y}; \omega). \tag{5}$$

The isovector dipole response, denoted henceforth as $S_L(q, \omega)$, may now be extracted from the imaginary part of a suitable polarization tensor. That is,

$$S_L(q, \omega) = -\frac{1}{\pi} \Im\, \Pi^{00}_{33}(\mathbf{q}, \mathbf{q}; \omega), \tag{6}$$

where the above labels refer to the isovector-timelike operator of Eq. (4) and $\Pi^{00}_{33}(\mathbf{q}, \mathbf{q}'; \omega)$ denotes the Fourier transform of $\Pi^{00}_{33}(\mathbf{x}, \mathbf{y}; \omega)$. Such an operator is capable of exciting all natural-parity states. To isolate the isovector dipole response one must project out the $(J^\pi = 1^-; T = 1)$ component of the polarization tensor. Thus, a transition operator of the following form is used:

$$\widehat{D}^0_{1\mu;3}(q, \mathbf{r}) = j_1(qr) Y_{1\mu}(\hat{\mathbf{r}}) \gamma^0 \tau_3 \underset{(qr \ll 1)}{\longrightarrow} \tfrac{1}{3} qr\, Y_{1\mu}(\hat{\mathbf{r}}) \gamma^0 \tau_3. \tag{7}$$

In the mean-field approximation the nuclear polarization tensor may be written exclusively in terms of the nucleon mean-field propagator $G_{\rm MF}(x, y)$ as follows:

$$i\,\Pi^{\alpha\beta}_{\rm MF}(x, y) = {\rm Tr}[\Gamma^\alpha G_{\rm MF}(x, y) \Gamma^\beta G_{\rm MF}(y, x)], \tag{8}$$

where the nucleon propagator $G^{\alpha\beta}_{\rm MF}$ is defined, in analogy to Eq. (2), as a time-ordered product of two nucleon fields

$$i G^{\alpha\beta}_{\rm MF}(x, y) = \langle \Phi_0 | T[\psi^\alpha(x) \bar{\psi}^\beta(y)] | \Phi_0 \rangle. \tag{9}$$

What defines the mean-field propagator is the replacement of the exact ground state of the system Ψ_0 by its mean-field approximation Φ_0. In the mean-field approximation the spectral content of the polarization tensor is both simple and illuminating [47]. The polarization tensor is an analytic function of the excitation energy ω—except for simple poles located at the one-particle–one-hole excitations of the mean-field system, with the residues at the individual poles yielding the transition form-factors.

To build collectivity into the nuclear response, all single-particle excitations of the same spin and parity must be mixed via a residual particle-hole interaction. The collective response of the system to an external perturbation is then obtained as a solution of the following set of RPA (Dyson's) equations [47]:

$$\Pi^{\alpha\beta}_{\rm RPA}(\mathbf{q}, \mathbf{q}'; \omega) = \Pi^{\alpha\beta}_{\rm MF}(\mathbf{q}, \mathbf{q}'; \omega) + \int \frac{d^3k}{(2\pi)^3} \frac{d^3k'}{(2\pi)^3} \times \Pi^{\alpha\lambda}_{\rm MF}(\mathbf{q}, \mathbf{k}; \omega) V_{\lambda\sigma}(\mathbf{k}, \mathbf{k}'; \omega) \times \Pi^{\sigma\beta}_{\rm RPA}(\mathbf{k}', \mathbf{q}'; \omega), \tag{10}$$

where $V_{\lambda\sigma}(\mathbf{k}, \mathbf{k}'; \omega)$ is the (momentum-space) residual particle-hole interaction. It should be stressed that to preserve important symmetries of the problem, the residual interaction must be consistent with the interaction used to generate the mean-field ground state [39,45]. Note that as certain symmetries of the infinite system are broken in the finite nucleus, the above set of integral equations becomes a complicated one. For example, the lack of translational invariance induces the mixing between various Lorentz structures (e.g., timelike and spacelike). Further, as the mean-field ground state is not isospin symmetric, isoscalar and isovector modes will also get mixed.

III. RESULTS

We start this section by displaying in Figs. 2 and 3 the distribution of isovector dipole strength for various members of the Sn-isotopic chain. (The distribution of strength in ^{132}Sn is shown in Fig. 7). In all cases the nuclear response is reported at the small momentum transfer of $q = 0.018$ fm^{-1} and includes a small artificial width of $\eta = 0.5$ MeV. An artificial width is included to resolve individual bound-state transitions; because

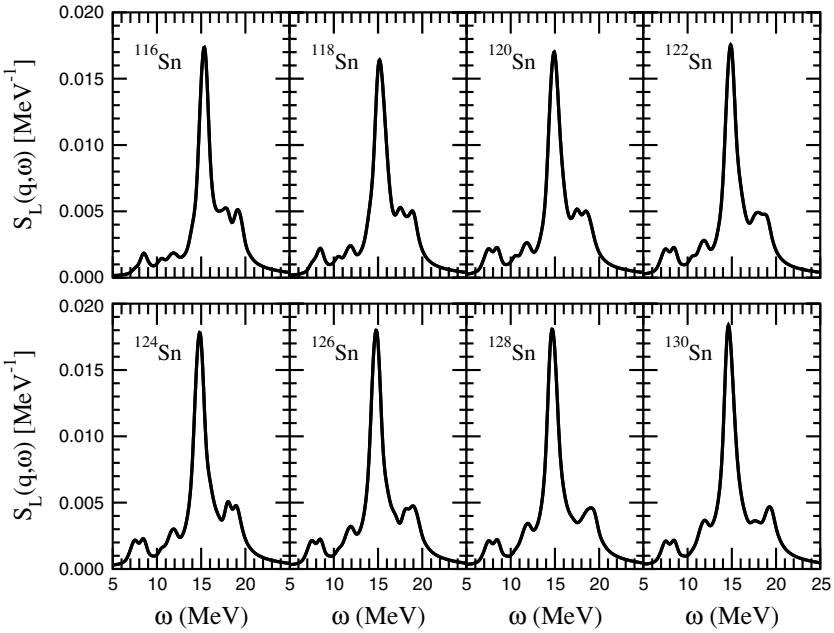

FIG. 3. Distribution of isovector dipole strength for all neutron-even tin isotopes from ^{116}Sn to ^{130}Sn at a momentum transfer of $q = 0.018$ fm^{-1}. All calculations include a small artificial width of $\eta = 0.5$ MeV and use the FSUGold parameter set [38].

of the nonspectral character of our calculation, particle-escape widths are computed exactly within the model.

The large collective structure in the $\omega \sim 15-16$ MeV region corresponds to the quintessential nuclear mode: the isovector giant dipole resonance (GDR). For medium-to-heavy nuclei, this collective vibration represents a coherent oscillation of all protons against all neutrons and is well-developed along the whole isotopic chain [48,49]. As is characteristic of these collective excitations, a large fraction of the energy-weighted sum rule is exhausted by this one resonance. But not all! The development of low-energy ($\omega \sim 7-9$ MeV) dipole strength with increasing neutron number is clearly discerned in Figs. 2 and 3. The progressive addition of "valence" neutrons—those occupying the $1g^{7/2}$, $2d^{5/2}$, $2d^{3/2}$, $3s^{1/2}$, and $1h^{11/2}$ orbitals (in that precise order)—results in a well-developed, albeit small, low-energy resonance. This oscillation of the excess neutrons—the neutron skin—against the isospin-symmetric core has been dubbed the PDR. In addition to the full distribution of isovector dipole strength, some of its moments have been tabulated in Table III. To do so, an ad hoc division was made at 10 MeV—with the PDR comprising the 5- to 10-MeV low-energy region and the GDR the 10- to 25-MeV high-energy region. Note that only PDR moments that account for at least 1% of the energy-weighted sum rule are tabulated.

We now turn to the first of the two questions posed in the Introduction: is there a strong correlation between the development of a neutron skin and the emergence of low-energy isovector dipole strength in the tin isotopes? To answer this question we have plotted in Fig. 4 the fraction of the energy-weighted sum rule contained in the PDR relative to that located in the GDR region [$\mathcal{M}_1 \equiv m_1(\mathrm{PDR})/m_1(\mathrm{GDR})$] as a function of the neutron skin ($R_n - R_p$). The same information may be found in tabular form in Tables I and III. Note that for those light isotopes for which the neutron skin is negative, $\mathcal{M}_1$ is (as expected) vanishingly small. Figure 4 displays a strong (almost linear) correlation between $\mathcal{M}_1$ and $R_n - R_p$ for $A \leqslant 120$. This lends support to the picture of the pygmy dipole resonance as an oscillation of the excess neutrons in the skin against the isospin-symmetric core. Yet as the neutron skin continues to increase in going from ^{120}Sn to ^{132}Sn, a mild anticorrelation actually develops. To elucidate these correlations it is useful to call on the single-particle (or mean-field) response.

The mean-field (or single-particle) isovector dipole response of both ^{120}Sn and ^{132}Sn are displayed on the left-hand panel of Fig. 5. To resolve most individual particle-hole

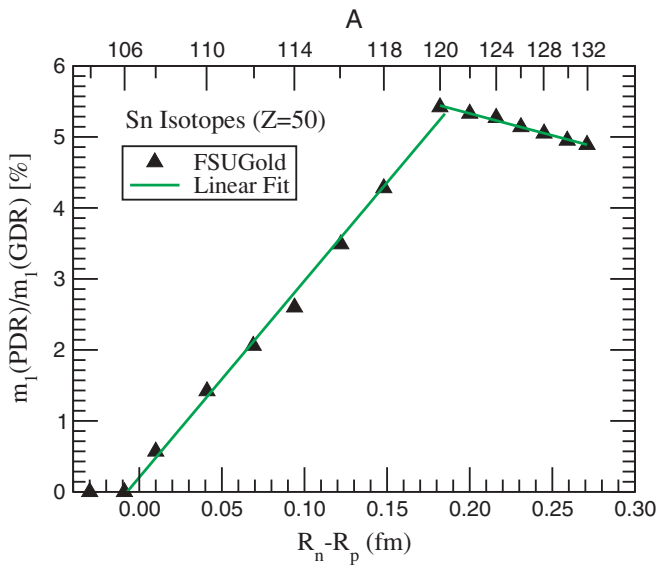

FIG. 4. (Color online) Fraction of the energy-weighted sum rule contained in the low-energy region (5−10 MeV) relative to that in the high-energy region (10−25 MeV) as a function of the neutron skin of the various Sn-isotopes.

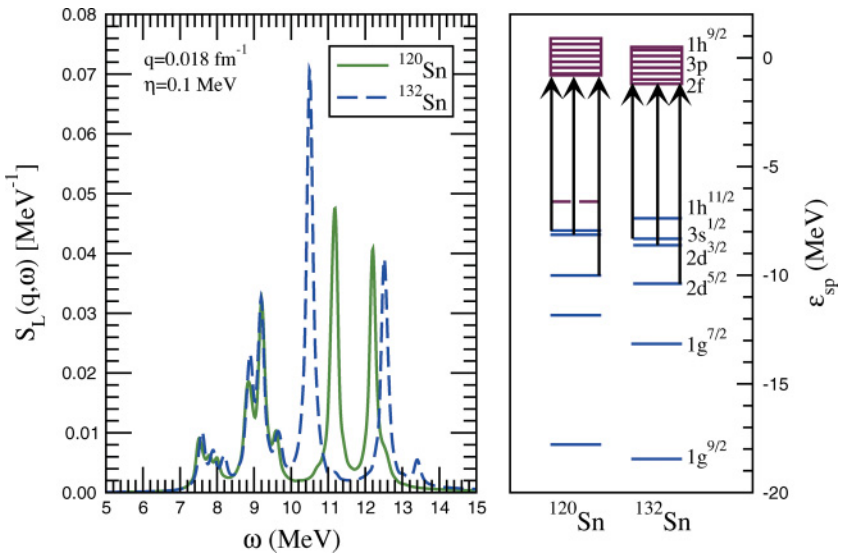

FIG. 5. (Color online) The left-hand panel displays the mean-field distribution of isovector dipole strength for ^{120}Sn and ^{132}Sn at a momentum transfer of $q = 0.018\ \mathrm{fm}^{-1}$. The calculations include a small artificial width of $\eta = 0.1$ MeV and use the FSUGold parameter set [38]. The right-hand panel depicts the allowed neutron transitions in the low-energy range.

transitions the artificial width has been reduced from $\eta = 0.5$ MeV to $\eta = 0.1$ MeV. The arrows on the right-hand panel indicate all relevant low-energy ($\omega \lesssim 10$ MeV) neutron excitations; no proton transitions are possible in this energy range. Some of these excitations involve states that are not bound (such as the $2f^{5/2}$ and $1h^{9/2}$), yet they are close enough in the continuum to produce relatively sharp peaks. Two sets of single-neutron transitions are clearly discernible in the $\omega \sim 7-8$ MeV and $\omega \sim 9-10$ MeV energy regions—with their mixing resulting in the "two-hump" PDR structure observed in the RPA response (see Fig. 3). What is significant, however, is that although the $1h^{11/2}$ neutron orbital gets filled in going from ^{120}Sn to ^{132}Sn, the low-energy structure of the single-particle response remains unchanged. This indicates that high-angular momentum orbitals play a passive role in driving low-energy transitions of low multipolarity. As the main GDR peak becomes more collective with increasing neutron number (see Table III), the fraction of the energy-weighted sum rule contained in the PDR peak actually goes down as the neutron skin continues to increase, thereby generating the weak anticorrelation displayed in Fig. 4.

We close the discussion on the first of the two questions posed in the Introduction by displaying in Fig. 6 the transition form factor $F^2_{\mathrm{PDR}}(q)$ associated with the pygmy dipole resonance. Note that (the square root of) this observable is directly related to the transition density. The transition form factor quantifies the efficiency of a probe that has inelastically scattered through a momentum transfer q in

TABLE III. Various moments of the isovector dipole distribution. The division between low-energy (pygmy) and high-energy (giant) dipole strength was made arbitrarily at 10 MeV.

A	Pygmy dipole resonance (PDR)			Giant dipole resonance (GDR)			PDR/GDR	
	$m_0(10^{-2})$	$m_1(10^{-2}$ MeV)	E_c (MeV)	$m_0(10^{-2})$	m_1 (MeV)	E_c (MeV)	m_0 (%)	m_1 (%)
100	—	—	—	4.58	0.79	17.22	—	—
102	—	—	—	4.70	0.81	17.17	—	—
104	—	—	—	4.81	0.82	17.11	—	—
106	—	—	—	4.91	0.84	17.06	—	—
108	—	—	—	5.01	0.85	17.00	—	—
110	0.14	1.23	8.51	5.12	0.86	16.85	2.81	1.42
112	0.21	1.81	8.51	5.25	0.88	16.69	4.05	2.06
114	0.27	2.30	8.49	5.37	0.89	16.52	5.08	2.60
116	0.38	3.12	8.30	5.48	0.89	16.31	6.87	3.49
118	0.47	3.86	8.21	5.60	0.90	16.10	8.40	4.28
120	0.62	4.92	7.94	5.70	0.91	15.90	10.86	5.42
122	0.62	4.89	7.93	5.78	0.92	15.88	10.66	5.33
124	0.62	4.90	7.93	5.87	0.93	15.86	10.53	5.27
126	0.61	4.84	7.92	5.95	0.94	15.84	10.27	5.14
128	0.61	4.81	7.91	6.03	0.95	15.80	10.08	5.05
130	0.60	4.77	7.91	6.11	0.96	15.78	9.88	4.95
132	0.60	4.77	7.90	6.20	0.98	15.74	9.73	4.89

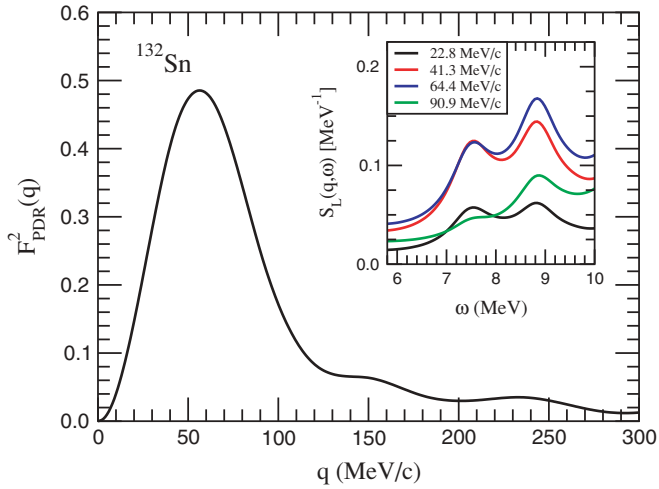

FIG. 6. (Color online) The transition form factor $F^2_{\rm PDR}(q)$ for the pygmy dipole resonance as a function of the momentum transfer to the nucleus q, extracted from integrating the isovector dipole response from 5 to 10 MeV. The inset is meant to illustrate the momentum-transfer dependence of the pygmy dipole strength.

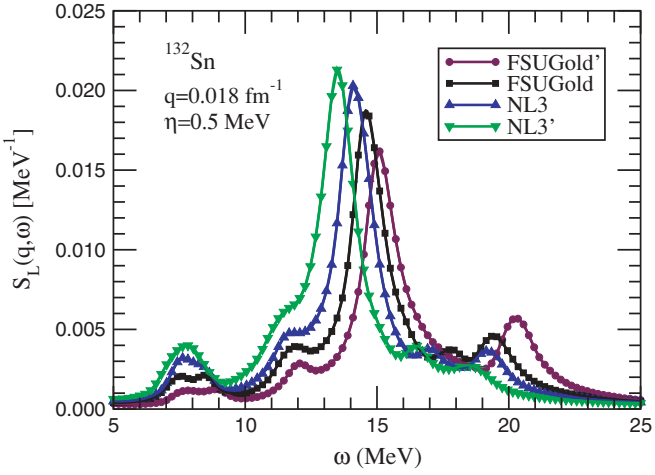

FIG. 7. (Color online) Model dependence of the distribution of isovector dipole strength in ^{132}Sn at a momentum transfer of $q = 0.018$ fm^{-1} and with a small artificial width of $\eta = 0.5$ MeV.

exciting the resonance. As the PDR is not sharp, the transition form factor—i.e., the residue at the pole—is extracted by integrating the (unweighted) isovector dipole response from $\omega_{\rm min} = 5$ MeV to $\omega_{\rm max} = 10$ MeV. This is schematically illustrated in the inset of Fig. 6 for a few values of the momentum transfer q. The transition form factor $F^2_{\rm PDR}(q)$ vanishes quadratically for small values of q, grows to its maximum value at a momentum transfer of the order of $q \simeq 60$ MeV/c, and decreases (with some modulation) for larger values of q. The low-q behavior is a simple consequence of Eq. (7). The large-q behavior, however, is model dependent and probes the nucleon momentum distribution. For a soft dipole oscillation (such as the PDR) that is driven by particle-hole states lacking high-momentum components, the falloff of the form factor with momentum transfer is thus relatively fast.

Having answered the first question posed in the Introduction, we now turn to the second and final one, namely could one use the recently measured isovector dipole strength in ^{130}Sn and ^{132}Sn [25] to discriminate among theoretical models that, although accurately calibrated, yield different predictions for the neutron skin of heavy nuclei. To address this question we introduce—in addition to FSUGold—three other parameter sets. One of these is the NL3 parameter set [36,37] used earlier to compute ground-state properties of the Sn isotopes (see Table I). Although enormously successful, NL3 predicts considerably larger neutron skins than FSUGold (see Tables I and IV). This is a result of its stiff symmetry energy—a property that at present is poorly determined by existent ground-state data. The remaining two sets (labeled FSUGold′ and NL3′), although themselves not calibrated by ground-state data, they are close "descendants" of FSUGold and NL3—aimed at further softening the symmetry energy of the former and stiffening the symmetry energy of the latter. To generate these two extra sets we followed a prescription first outlined in Ref. [8] that preserves the value of the symmetry-energy coefficient at a density that is slightly below nuclear-matter saturation density. This prescription ensures

TABLE IV. Model dependence of the neutron skins, PDR centroid energies, GDR centroid energies, and PDR-to-GDR m_1 ratios for ^{130}Sn and ^{132}Sn. Experimental data is from Ref. [25].

Nucleus	Model	$R_n - R_p$ (fm)	PDR E_c (MeV)	GDR E_c (MeV)	PDR/GDR m_1(%)
^{130}Sn	FSUGold′	0.180	7.94	16.42	3.38
	FSUGold	0.259	7.91	15.78	4.95
	NL3	0.330	7.91	15.13	6.49
	NL3′	0.415	7.84	14.47	8.70
	Experiment	—	10.1(7)	15.9(5)	5(2)
^{132}Sn	FSUGold′	0.189	8.01	16.59	3.04
	FSUGold	0.271	7.90	15.74	4.89
	NL3	0.346	7.90	15.08	6.44
	NL3′	0.432	7.85	14.36	8.69
	Experiment	—	9.8(7)	16.1(7)	3(2)

that the density dependence of the symmetry energy is modified without compromising the success of the model in reproducing well-constrained ground-state observables. By introducing these parameter sets, we have been able to generate a wide range of values for the neutron skin of ^{130}Sn and ^{132}Sn (see Table IV). Note, however, that in the case of FSUGold′, a minor rescaling (of less than 0.5%) of the isoscalar-scalar mass (m_s) was required to ensure the same proton radius in ^{132}Sn for all four models.

The distribution of isovector dipole strength for the exotic, neutron-rich isotope ^{132}Sn is displayed in Fig. 7. As in all previous figures, the nuclear response is displayed at the small momentum transfer of $q = 0.018$ fm^{-1} and includes an artificial width of $\eta = 0.5$ MeV. In addition, neutron skins, centroid energies $E_c \equiv m_1/m_0$, and PDR-to-GDR m_1 ratios for both ^{130}Sn and ^{132}Sn are listed in Table IV. Whenever possible, these observables are compared against the recently available experimental data [25]. Perhaps surprisingly, the centroid energy of the PDR is largely insensitive to the neutron skin. Yet there is a noticeable enhancement with increasing neutron skin of the fraction of the energy-weighted sum rule located at low energies. Although the experimental error bars are large, the data seem to disfavor models with overly large neutron skins. We regard this result as an important and gratifying consistency check. In recent theoretical studies of the IVGDR in ^{208}Pb, it was already suggested that models with a stiff symmetry energy—and thereby large neutron skins—underpredict the location of the peak [19,20]. Not surprisingly, the same trend is observed here: models with a stiff symmetry energy, such as NL3 and even more so NL3′, predict GDR centroid energies in both ^{130}Sn and ^{132}Sn that are low relative to experiment.

We conclude this section with a comment addressing the apparent discrepancy between theory and experiment on the location of the PDR centroid energy. We find a substantial amount of low-energy strength in bound excitations, an identification that is in agreement with earlier studies [32,34]. For example, all mean-field strength located in the $\omega \lesssim 8$ MeV region corresponds to bound-state transitions of the form $3s^{1/2} \rightarrow [3p^{3/2}, 3p^{1/2}]$; $2d^{3/2} \rightarrow [3p^{3/2}, 3p^{1/2}]$, and so on (see Fig. 5). Further, most (although not all) of the strength found in the $\omega \simeq 8.5-10$ MeV region also involves transitions to bound states. Yet experimentally, only isovector dipole strength above the one-neutron separation energy was detected [25]. Naturally, this tends to shift the centroid energy of the PDR to higher energies. In an effort to simulate the experimental conditions, we have turned off the artificial width in our calculations (from $\eta = 0.5 \rightarrow 0$ MeV), thereby eliminating all bound-state transitions. Implementing this procedure results in a shift of the PDR centroid energy in ^{132}Sn from $E_c = 7.90$ MeV to $E_c \simeq 9.40$ MeV, well within experimental error.

IV. CONCLUSIONS

Motivated by the first experimental measurement of isovector dipole strength in the two exotic, neutron-rich isotopes ^{130}Sn and ^{132}Sn, the theoretical response along the full (neutron-even) isotopic chain was studied via a relativistic MF+RPA approach. Particular emphasis was placed on the pygmy dipole resonance, an oscillation of the excess neutrons in the skin against the isospin-symmetric core. Our study was shaped by two underlying questions: (a) is there a correlation between the development of a neutron skin and the emergence of low-energy isovector dipole strength? and (b) can the experimental data be used to discriminate among models that, although accurately calibrated, predict different values for the neutron skin of heavy nuclei?

We found that the answer to the first question was not unique. Although a strong linear correlation between the neutron skin and the fraction of the energy-weighted sum rule at low energies was indeed observed, a mild anticorrelation actually developed beyond ^{120}Sn. The emergence of this anticorrelation was attributed to the $1h^{11/2}$ neutron orbital. Although this orbital contributes significantly to the size of the neutron skin, its large angular momentum hinders its participation in low-energy transitions of low multipolarity.

The answer to the second question yielded various insights. First, the centroid energy of the PDR was found to be insensitive to the density dependence of the symmetry energy. That is, theoretical models that predict neutron skins in ^{132}Sn that vary by more than a factor of 2, yield centroid energies within 2% of each other. Yet these narrowly spread centroid energies are about 2 MeV lower than experiment. This discrepancy was attributed to the fact that the observed experimental strength lies above the one-neutron separation energy. To simulate this experimental condition, we suppressed all bound-state transitions by turning off the artificial width from our calculations. In accordance with experimental observations, the centroid energy increased by 1.5 MeV. Finally, the fraction of the energy-weighed sum rule exhausted by the PDR was observed to increase sharply with increasing neutron skin, from 3% for the model with the softest symmetry energy to almost 9% for the model with the stiffest one. In spite of the relatively large experimental error bars, the data seems to disfavor models with an overly stiff symmetry energy. This result adds to the already large body of evidence supporting a symmetry energy with a soft density dependence [11,38,50,51].

We conclude with a few comments on the impact of the pygmy dipole resonance on various astrophysical phenomena. As already mentioned, the systematics of this mode may be used to constrain the density dependence of the symmetry energy, a property that has a strong impact on a variety of neutron-star properties, such as its composition, radius, and cooling mechanism [7–9]. Further, the presence of low-energy dipole strength in neutron-rich nuclei significantly enhances the cross section for the radiative capture of low-energy ($\sim$10 MeV) neutrons [52,53], a process of fundamental importance to the creation of the heavy elements by means of the rapid neutron capture process [54]. Finally, the existence of a pygmy dipole resonance in neutron-rich nuclei may aid the supernovae explosion mechanism. In a supernovae explosion 99% of the energy of the collapse is radiated away in neutrinos. Neutrinos interact strongly with neutrons because of the large weak vector charge of the neutron. Supernovae neutrinos may then couple strongly to the neutron-rich skin and excite the

low-energy modes of the many exotic nuclei ("pasta") present in this explosive environment [55]. This may allow for a significant energy transfer to the nuclear medium, potentially reviving the stalled supernovae shock.

ACKNOWLEDGMENTS

This work was supported in part by DOE grant DE-FG05-92ER40750.

[1] B. G. Todd and J. Piekarewicz, Phys. Rev. C **67**, 044317 (2003).
[2] S. J. Pollock, E. N. Fortson, and L. Wilets, Phys. Rev. C **46**, 2587 (1992).
[3] B. A. Brown, Phys. Rev. Lett. **85**, 5296 (2000).
[4] M. B. Tsang *et al*., Phys. Rev. Lett. **92**, 062701 (2004).
[5] L.-W. Chen, C. M. Ko, and B.-A. Li, Phys. Rev. Lett. **94**, 032701 (2005).
[6] A. W. Steiner and B.-A. Li, Phys. Rev. C **72**, 041601(R) (2005).
[7] C. J. Horowitz and J. Piekarewicz, Phys. Rev. Lett. **86**, 5647 (2001).
[8] C. J. Horowitz and J. Piekarewicz, Phys. Rev. C **64**, 062802(R) (2001).
[9] C. J. Horowitz and J. Piekarewicz, Phys. Rev. C **66**, 055803 (2002).
[10] A. W. Steiner, M. Prakash, J. M. Lattimer, and P. J. Ellis, Phys. Rep. **411**, 325 (2005).
[11] B.-A. Li and A. W. Steiner (2005), nucl-th/0511064.
[12] L. Ray and G. W. Hoffmann, Phys. Rev. C **31**, 538 (1985).
[13] L. Ray, G. W. Hoffmann, and W. R. Coker, Phys. Rep. **212**, 223 (1992).
[14] G. Fricke, C. Bernhardt, K. Heilig, L. A. Schaller, L. Schellenberg, E. B. Shera, and C. W. de Jager, At. Data Nucl. Data Tables **60**, 177 (1995).
[15] C. J. Horowitz, S. J. Pollock, P. A. Souder, and R. Michaels, Phys. Rev. C **63**, 025501 (2001).
[16] K. A. Aniol *et al*. (HAPPEX Collaboration), Phys. Rev. Lett. **96**, 022003 (2006).
[17] K. A. Aniol *et al*. (HAPPEX Collaboration) (2005), nucl-ex/0506011.
[18] R. Michaels, P. A. Souder, and G. M. Urciuoli (2005), http://hallaweb.jlab.org/parity/prex.
[19] J. Piekarewicz, Phys. Rev. C **69**, 041301(R) (2004).
[20] D. Vretenar, T. Niksic, and P. Ring, Phys. Rev. C **68**, 024310 (2003).
[21] J. Piekarewicz, Phys. Rev. C **66**, 034305 (2002).
[22] B. K. Agrawal, S. Shlomo, and V. K. Au, Phys. Rev. C **68**, 031304 (2003).
[23] G. Colo, N. Van Giai, J. Meyer, K. Bennaceur, and P. Bonche, Phys. Rev. C **70**, 024307 (2004).
[24] R. J. Furnstahl, Nucl. Phys. **A706**, 85 (2002).
[25] P. Adrich *et al*., Phys. Rev. Lett. **95**, 132501 (2005).
[26] Y. Suzuki, K. Ikeda, and H. Sato, Prog. Theor. Phys. **83**, 180 (1990).
[27] P. Van Isacker, M. A. Nagarajan, and D. D. Warner, Phys. Rev. C **45**, R13 (1992).
[28] D. Vretenar, N. Paar, P. Ring, and G. A. Lalazissis, Phys. Rev. C **63**, 047301 (2001).
[29] D. Vretenar, N. Paar, P. Ring, and G. A. Lalazissis, Nucl. Phys. **A692**, 496 (2001).
[30] I. Hamamoto, H. Sagawa, and X. Z. Zhang, Phys. Rev. C **53**, 765 (1996).
[31] I. Hamamoto, H. Sagawa, and X. Z. Zhang, Phys. Rev. C **57**, R1064 (1998).
[32] N. Paar, P. Ring, T. Niksic, and D. Vretenar, Phys. Rev. C **67**, 034312 (2003).
[33] N. Tsoneva, H. Lenske, and C. Stoyanov, Phys. Lett. **B586**, 213 (2004).
[34] D. Sarchi, P. F. Bortignon, and G. Colo, Phys. Lett. **B601**, 27 (2004).
[35] N. Paar, T. Niksic, D. Vretenar, and P. Ring, Phys. Lett. **B606**, 288 (2005).
[36] G. A. Lalazissis, J. Konig, and P. Ring, Phys. Rev. C **55**, 540 (1997).
[37] G. A. Lalazissis, S. Raman, and P. Ring, At. Data Nucl. Data Tables **71**, 1 (1999).
[38] B. G. Todd-Rutel and J. Piekarewicz, Phys. Rev. Lett. **95**, 122501 (2005).
[39] J. Piekarewicz, Phys. Rev. C **64**, 024307 (2001).
[40] B. D. Serot and J. D. Walecka, Adv. Nucl. Phys. **16**, 1 (1986).
[41] B. D. Serot and J. D. Walecka, Int. J. Mod. Phys. E **6**, 515 (1997).
[42] H. Mueller and B. D. Serot, Nucl. Phys. **A606**, 508 (1996).
[43] C. W. De Jager, H. De Vries, and C. De Vries, At. Data Nucl. Data Tables **36**, 495 (1987).
[44] G. Audi and A. H. Wapstra, Nucl. Phys. **A595**, 409 (1995).
[45] J. F. Dawson and R. J. Furnstahl, Phys. Rev. C **42**, 2009 (1990).
[46] J. D. Bjorken and S. D. Drell, *Relativistic Quantum Mechanics* (McGraw-Hill, New York, 1964).
[47] A. L. Fetter and J. D. Walecka, *Quantum Theory of Many Particle Systems* (McGraw-Hill, New York, 1971).
[48] G. F. Bertsch and R. A. Broglia, *Oscillations in Finite Quantum Systems* (Cambridge University Press, Cambridge, 1994).
[49] M. N. Harakeh and A. van der Woude, *Giant Resonances: Fundamental High-Frequency Modes of Nuclear Excitation* (Clarendon, Oxford, 2001).
[50] L.-W. Chen, C. M. Ko, and B.-A. Li, Phys. Rev. C **72**, 064309 (2005).
[51] D. V. Shetty, S. J. Yennello, and G. A. Souliotis (2005), nucl-ex/0505011.
[52] S. Goriely and E. Khan, Nucl. Phys. **A706**, 217 (2002).
[53] S. Goriely, E. Khan, and M. Samyn, Nucl. Phys. **A739**, 331 (2004).
[54] S. Goriely, Phys. Lett. **B436**, 10 (1998).
[55] C. J. Horowitz, M. A. Perez-Garcia, D. K. Berry, and J. Piekarewicz, Phys. Rev. C **72**, 035801 (2005).